Reconstruction of a daily gridded snow water equivalent product for the land region above 45° N based on a ridge regression machine learning approach

Donghang Shao[1,2], Hongyi Li[1,2], Jian Wang[1,2], Xiaohua Hao[1,2], Tao Che[1,2] and Wenzheng Ji[1,2,3]

[1]Northwest Institute of Eco-Environment and Resources, Chinese Academy of Sciences, Lanzhou, 730000, China

[2]Heihe Remote Sensing Experimental Research Station, Key Laboratory of Remote Sensing of Gansu Province, Chinese Academy of Sciences, Lanzhou, 730000, China

[3]University of Chinese Academy of Sciences, Beijing, 100049, China

Correspondence to: Hongyi Li (lihongyi@lzb.ac.cn)

Abstract. The snow water equivalent (SWE) is an important parameter of surface hydrological and climate systems, and it has a profound impact on Arctic amplification and climate change. However, there are great differences among existing SWE products. In the land region above 45° N, the existing SWE products are associated with a limited time span and limited spatial coverage, and the spatial resolution is coarse, which greatly limits the application of SWE data in cryosphere change and climate change studies. In this study, utilizing the ridge regression model (RRM) of a machine learning algorithm, we integrated various existing SWE products to generate a spatiotemporally seamless and high-precision RRM SWE product. The results show that it is feasible to utilize a ridge regression model based on a machine learning algorithm to prepare SWE products on a global scale. We evaluated the accuracy of the RRM SWE product using hemispheric-scale snow course (HSSC) observational data and Russian snow survey data. The MAE, RMSE, R, and R² between the RRM SWE products and observed SWEs are 0.21, 25.37 mm, 0.89, and 0.79, respectively. The accuracy of the RRM SWE dataset is improved by 28%, 22%, 37%, 11%, and 11% compared with the original AMSR-E/AMSR2 (SWE), ERA-Interim SWE, Global Land Data Assimilation System (GLDAS) SWE, GlobSnow SWE, and ERA5-land SWE datasets, respectively, and it has a higher spatial resolution. The RRM SWE product production method does not rely heavily on an independent SWE product; it takes full advantage of each SWE dataset, and it takes into consideration the altitude factor. The MAE ranges from 0.16 for areas within <100 m elevation to 0.29 within the 800-900 m elevation range. The MAE is best in the Russian region and worst in

the Canadian region. The RMSE ranges from 4.71 mm for areas within <100 m elevation to 31.14 mm within the >1000 m elevation range. The RMSE is best in the Finland region and worst in the Canadian region. This method has good stability, is extremely suitable for the production of snow datasets with large spatial scales, and can be easily extended to the preparation of other snow datasets. The RRM SWE product is expected to provide more accurate SWE data for the hydrological model and climate model and provide data support for cryosphere change and climate change studies. The RRM SWE product is available from 'A Big Earth Data Platform for Three Poles' (http://dx.doi.org/10.11888/Snow.tpdc.271556) (Li et al., 2021).

1 Introduction

The IPCC (Intergovernmental Panel on Climate Change) AR6 (Sixth Assessment Report) notes that the Northern Hemisphere spring snow cover has greatly decreased since 1950, and the feedback effect of the climate system caused by this reduction is extremely large (Masson-Delmotte et al., 2021). In most land areas of the Northern Hemisphere, annual runoff is dominated by snowmelt, and accurately estimating the impacts of such a large amount of snowmelt runoff on ecosystems and human activities is of great significance (Barnett et al., 2005; Bintanja and Andry, 2017; Henderson et al., 2018). Whether through hydrometeorological simulation or global change research, the estimation of the energy budget and mass of snow is very difficult, so a set of highly accurate, long time series snow cover datasets is urgently needed to drive hydrometeorological simulations and land surface process models. Among them, snow water equivalent (SWE) data play an irreplaceable role as an important parameter of the land surface hydrological model and climate model.

At present, there are many forms of SWE data in the world. According to type, these data can be divided into site observational SWE, remote sensing SWE, reanalysis SWE, data assimilation SWE and model simulation SWE. The remote sensing SWEs are mainly AMSR-E (Kelly, 2009) and AMSR2 (Imaoka et al., 2010; Tedesco and Jeyaratnam, 2019). The reanalysis SWE was mainly based on the ERA-Interim (Dee et al., 2011), MERRA2 (Gelaro et al., 2017), MERRA land (Reichle et al., 2011), and ERA5-land (Muñoz Sabater, 2019; Balsamo et al., 2015) datasets. The data assimilation SWE mainly includes GlobSnow (Luojus et al., 2021) and the Global Land Data Assimilation System (GLDAS) (Rodell et al., 2004). The site observational SWE mainly includes the GHCN dataset (Menne et al., 2016) and HSSC data (Pulliainen et al.,

48 2020). However, the time ranges of AMSR-E and AMSR-E2 SWE are only from 2003 to the present, which is lacking in

49 terms of time series. Similarly, the GlobSnow SWE dataset is also seriously lacking in time series. Although the reanalysis

50 SWE data have good spatial and temporal continuity and high data integrity, their accuracy is poor, and the MAE is 0.65

51 (Snauffer et al., 2016). The SWE data from stations and meteorological observations cannot meet the needs of

52 hydrometeorological and climate change research. This is mainly because SWE from stations is discontinuous in time series

53 and severely missing. Furthermore, hydrometeorological studies often require spatiotemporally continuous grid data to be

54 derived (Pan et al., 2003). There are great differences among remote-sensing SWE, reanalysis SWE data, data assimilation

55 SWE and observational SWE. For remote-sensing SWE, the spatiotemporal characteristics of different passive microwave

56 SWE data differ significantly due to differences in sensors or retrieval algorithms (Mudryk et al., 2015a). Data assimilation

57 SWE and reanalysis SWE data also tend to exhibit different spatiotemporal characteristics due to differences in model

58 design, driving data, and assimilation methods (Vuyovich et al., 2014). In summary, although there are a variety of SWE data

59 in the world, the data quality is uncertain.

60   Previous studies have shown that all kinds of SWE data in the Northern Hemisphere have advantages and disadvantages,

61 and none of these data perform well in all aspects (Mortimer et al., 2020). An effective method was applied in a study by

62 Pulliainen et al. (Pulliainen et al., 2020), who applied a bias correction to GlobSnow and reanalysis data products based on

63 SWE snow course measurements to obtain improved estimates on annual peak snow mass and SWE in the Northern

64 Hemisphere. Another effective method is to fuse all kinds of SWE data in time and space, integrate the advantages of all

65 kinds of data, and then generate a relatively complete SWE dataset. Many scholars have conducted in-depth studies on SWE

66 data fusion. The main fusion methods can be classified into the following categories: multiproduct direct averaging (Mudryk

67 et al., 2015b), linear regression (Snauffer et al., 2016), data assimilation (Pulliainen, 2006), "multiple" collocation (Pan et al.,

68 2015) and machine learning (Snauffer et al., 2018; Xiao et al., 2018; Wang et al., 2020). Studies have shown that even the

69 simplest multisource data average is more accurate than a single SWE product (Snauffer et al., 2018). However, the simple

70 multisource data average cannot highlight the advantages of high-precision data, and it is easily affected by the weight ratio

71 of low-precision data, which reduces the accuracy of fused data (Mudryk et al., 2015a). Although the linear regression

72 method can make good use of the actual observational data to correct the original data, it is easy to overfit and causes the

overall deviation (Snauffer et al., 2016). The "multiple" collocation method changes the size of the original SWE data before fusion, which easily causes data errors. The data assimilation method is sensitive to the accuracy of input data, and it is difficult to fuse multisource data (Pan et al., 2015). In recent years, machine learning methods have been widely used in data fusion (Santi et al., 2021; Ntokas et al., 2021). Machine learning methods can not only integrate the advantages of multisource data but also make full use of site observational data to train the sample data, which easily generates SWE data products with large spatial scales and long time series (Broxton et al., 2019; Bair et al., 2018).

In summary, based on the existing SWE data products, combining a machine learning algorithm to fuse multisource SWE data is an effective method to prepare SWE products with long time series and large spatial scales and retain the advantages of single SWE data products. The ridge regression model is a biased estimation method specifically designed to address the problem of multicollinear data (Duzan and Shariff, 2015; Saleh et al., 2019). It has good tolerance to "ill-conditioned" data and has a good effect in using SWE data to address the multicollinearity problem (Hoerl and Kennard, 1970b; Guilkey and Murphy, 1975). In this study, we integrated multisource SWE data products of the RRM SWE based on the ridge regression model of the machine learning algorithm. We selected ERA-Interim SWE, GLDAS SWE, GlobSnow SWE, AMSR-E/AMSR2 SWE, and ERA5-land SWE data with relatively complete time series as the original data for the production of the RRM SWE product. The missing parts of the ERA-Interim SWE, AMSR-E/AMSR2 SWE, and GlobSnow SWE data were filled by the spatiotemporal interpolation method. The HSSC dataset (Pulliainen et al., 2020) and Russian snow survey data (Bulygina et al., 2011) were used as training sample data of "true SWE", and the effect of altitude on the algorithm was also considered. Thus, we prepared a set of spatiotemporal seamless SWE datasets (RRM SWE) covering the land region above 45° N from 1979 to 2019. The spatial coverage of the RRM SWE product covers all land regions north of 45° N.

2 Data and methods

2.1 Research region

The research region of the RRM SWE product is located in the land region north of 45° N (Fig. 1). This region consists of Asia, Europe, and North America. The land region covers Russia, the United States, Canada, Denmark, Norway, Iceland,

96 Sweden, and Finland. This region has a cold climate and a wide area of snow cover.

97 **2.2 Grid SWE data description**

98 In this study, we utilized ERA-Interim SWE data (Dee et al., 2011), GLDAS SWE data (Rodell et al., 2004), GlobSnow

99 SWE data (Luojus et al., 2021), AMSR-E/AMSR2 SWE data (Tedesco and Jeyaratnam, 2019), and ERA5-land SWE data

100 (Muñoz Sabater, 2019) as the original input datasets for the fusion data (Table 1).

101 GlobSnow is a dataset of global snow cover and SWEs for the Northern Hemisphere released by the European Space

102 Agency (ESA) (http://www.globsnow.info/swe/) (Luojus et al., 2021; Pulliainen et al., 2020). The SWE products in this

103 dataset combine the Canadian Meteorological Center (CMC) daily snow depth analysis data (Walker et al., 2011), ground

104 weather site observational data, and satellite microwave radiometer data. We obtained the L3A_daily_SWE product of this

105 dataset. The temporal resolution of the L3A_daily_SWE product is daily, the spatial resolution is 0.25°, and the data format

106 is NETCDF4.

107 ERA-Interim is the fourth generation reanalysis data of the European Centre for Medium-Range Weather Forecasts

108 (ECMWF) (Dee et al., 2011). The data provide a global assimilated numerical product of various surface and top

109 atmospheric parameters from January 1979 to the present (https://apps.ecmwf.int/datasets/data/interim-full-

110 daily/levtype=sfc/). We obtained the SWE dataset with a daily temporal resolution, a spatial resolution of 0.25°, and

111 NETCDF4 data format. The spatial range of the data is the land region above 45° N.

112 The Advanced Microwave Scanning Radiometer-Earth Observation System (AMSR-E) is a microwave scanning

113 radiometer on the Aqua satellite of the National Aeronautics and Space Administration (NASA) Earth Observation System

114 (EOS) (Tedesco and Jeyaratnam, 2019). The AMSR-E provides a global daily SWE dataset from June 19, 2002, to October

115 3, 2011 (https://nsidc.org/data/ae_dysno). AMSR2 is a microwave scanning radiometer on the GCOM-W1 satellite launched

116 by the Japan Aerospace Exploration Agency (JAXA) in May 2012. AMSR2 provides a global SWE dataset from July 2,

117 2012, to the present (https://nsidc.org/data/AU_DySno/versions/1). The spatial resolution of the AMSR-E SWE and AMSR2

118 SWE datasets is 25 km x 25 km, the temporal resolution is daily, and the data formats are HDF-EOS and HDF-EOS5,

119 respectively.

120   The GLDAS is a model used to describe global land information; it contains data, such as global rainfall, water

121   evaporation, surface runoff, underground runoff, soil moisture, surface snow cover distribution, temperature, and heat flow

122   distribution (Rodell et al., 2004). This assimilation system includes data with spatial resolutions of $1° \times 1°$ and $0.25° \times 0.25°$

123   and temporal resolutions of 3 hours, 1 day and 1 month. The GLDAS data are available for download from the Goddard

124   Earth Sciences Data and Information Services Center (GES DISC). We obtain an SWE dataset with a daily temporal

125   resolution, $0.25°$ spatial resolution, and NETCDF4 data format.

126   ERA5-land is a reanalysis dataset that provides the evolution of global land parameter data since 1981 (Muñoz Sabater,

127   2019). The dataset provides eight types of snow parameter data, including snow albedo, snow cover, snow depth, snowfall,

128   the temperature of the snow layer, snowmelt, snow density, and SWE. This dataset provides a global SWE dataset with an

129   hourly spatial resolution, a temporal resolution of $0.1° \times 0.1°$, a temporal coverage of January 1981 to the present, and data

130   formats of GRIB and NETCDF4.

131   To maintain consistency in the spatial and temporal resolutions of the fused data, we unified the ERA-Interim SWE data,

132   GLDAS SWE data, GlobSnow SWE data, AMSR-E/AMSR2 SWE data, and ERA5-land SWE data into a daily temporal

133   resolution, with a spatial resolution of $0.25°$ and geographic projection of the North Pole Lambert azimuthal equal area.

134   **2.3 Ridge regression machine learning algorithm for preparing the SWE**

135   In this study, we utilize the ridge regression model of a machine learning algorithm to fuse ERA-Interim SWE data (Dee et

136   al., 2011), GLDAS SWE data (Rodell et al., 2004), GlobSnow SWE data (Luojus et al., 2021), AMSR-E/AMSR2 SWE data

137   (Tedesco and Jeyaratnam, 2019), and ERA5-land SWE data (Muñoz Sabater, 2019) to generate a set of new RRM SWE

138   datasets. The target reference data in this study are the HSSC dataset and Russian snow survey data. The digital elevation

139   model (DEM) was used as an important environmental feature input to the ridge regression model and was included in the

140   model training. The DEM is an auxiliary terrain feature variable in addition to the five SWE prediction feature variables,

141   AMSR-E/AMSR2 SWE, ERA-Interim SWE, GLDAS SWE, GlobSnow SWE, and ERA5-land SWE.

142   The ridge regression model is a biased estimate regression method for collinear data analysis (Friedman et al., 2010; Hoerl

143   and Kennard, 1970b, a). By abandoning the unbiasedness of the ordinary least squares, this algorithm can obtain the

144   regression method in which the regression coefficient is more practical and reliable at the cost of losing part of the

145   information and reducing the accuracy. The ridge regression model is flexible in the choice of predictor variables and does

146   not require the predictor and target variables to be independent of each other. It can effectively solve the multicollinearity

147   problem of predictor and target variables as well as reduce the impact of this problem on the training model (Duzan and

148   Shariff, 2015; Saleh et al., 2019). Generally, reanalysis data based on SWE products cannot make the products and models

149   independent of each other, i.e., they are prone to multicollinearity, which leads to distorted model estimation or difficulty in

150   performing accurate estimations. In contrast, the ridge regression model can successfully solve the multicollinearity problem,

151   i.e., the independence of training products and models. In addition, when integrating multiple SWE products, the accuracy of

152   each SWE dataset is likely to differ. A small change in one of the SWE products involved in the training will cause a

153   significant error in the final calculation results, while the ridge regression model has high accuracy and stability for these

154   "ill-conditioned" SWE data. In addition, the main advantage of this model is that SWE products with long time series and

155   large spatial scales are easy to prepare. The principle equation of the ridge regression model is defined as follows:

156
$$\hat{\beta}^{ridge} = \underset{\beta}{\arg\min}\left\{\sum_{i=1}^{N}\left(y_i - \beta_0 - \sum_{j=1}^{p}x_{ij}\beta_j\right)^2 + \lambda\sum_{j=1}^{p}\beta_j^2\right\},$$
(1)

157   where $\hat{\beta}^{ridge}$ is the extremum solution function of ridge regression and p is the number of gridded SWE product variables

158   involved in training. x_i are the prediction feature variables, which contain two parts: one set contains the main feature

159   variables of the gridded SWE products, and the other part consists of the DEM auxiliary feature variables. y_i is the observed

160   SWE, and λ, β, β_j and β_0 are the parameters to be solved. $1, \cdots, N$ is the sample of the training dataset. $\lambda\sum_{j=1}^{p}\beta_j^2$ is the

161   penalty function term. The total number of samples N in the training dataset is 271651. The sample sizes of the training

162   dataset, validation dataset and test dataset are divided according to the ratio of 7:2:1, where the numbers of training set,

163   validation set and test set samples are 271651, 77614 and 38807, respectively. The model is developed in Python3, and the

164   model framework is based on the "scikit-learn" machine learning library (https://scikit-learn.org/stable/index.html). The code

165   is available upon request.

The integration process of the RRM SWE product (Fig. 2) is described as follows:

1) The original ERA-Interim SWE data, GLDAS SWE data, GlobSnow SWE data, AMSR-E/AMSR2 SWE data, ERA5-land SWE data, DEM data, unified temporal resolution, spatial resolution, projection, spatial range, and unit are preprocessed.

2) The spatiotemporal interpolation method is used to fill in the missing data of AMSR-E/AMSR2 SWE, ERA-Interim SWE, and GlobSnow SWE in space and time. Based on this method, the missing AMSR-E/AMSR2 SWE data at low latitudes and the missing ERA-Interim SWE and GlobSnow SWE data in the time series are added.

3) The SWE data observed at stations from 1979 to 2014 are used as sample training data, and the AMSR-E/AMSR2 SWE, ERA-Interim SWE, GLDAS SWE, GlobSnow SWE, ERA5-land SWE data, and DEM data are input into the ridge regression model of a machine learning algorithm for training. During the RRM model training process, we reconstructed the training data to try to extract training samples that are uniformly distributed spatially as much as possible. First, a scan window of 250 km × 250 km (10 × 10 pixels) was created. Then, each gridded SWE data point participating in training is scanned, and the sample numbers in each scan window are counted. Finally, the mean value n of the sample numbers in all scan windows is taken as the number of training samples to be selected in each scan window. For the scan window with sample numbers higher than n, n samples are randomly selected from the scan window. For the scan window with sample numbers lower than n, all samples in the scan window are selected as training samples.

4) When the model was trained, ERA-Interim SWE, GLDAS SWE, GlobSnow SWE, and ERA5-land SWE were used as the training data between 1979 and 2002 (AMSR-E/AMSR2 SWE data were not available before 2002), and AMSR-E/AMSR2 SWE, ERA-Interim SWE, GLDAS SWE, GlobSnow SWE, and ERA5-land SWE were used as the training data after 2002.

5) Based on the S-fold cross-validation method, the SWE data are continuously trained and validated, and the optimal model and parameters are finally selected and evaluated by the loss function.

6) Based on the trained optimal model, multiple SWE data products are integrated into the time series, missing data are predicted, and a set of spatiotemporally seamless SWE datasets is generated.

191   7)   SWE data observed at stations from 2015 to 2018 are used to evaluate the accuracy of the RRM SWE product.

192   **2.4 Site data and evaluation metrics**

193   **2.4.1 Site SWE data for training, validation, and testing**

194   Russian snow survey data (http://aisori.meteo.ru/ClimateR) include the average snow depth data and the average snow

195   density data of the station, and the SWE is the product of the measured average snow depth and average snow density

196   (Bulygina et al., 2011). We obtained SWE data from 19493 stations from 1979-2016 from this dataset.

197   Hemispheric-scale snow course (hereafter referred to as HSSC) observational data are contained in a hemispheric-scale

198   SWE database based on SWE observational datasets from the former Soviet Union/Russia (FSU), Finland, and Canada

199   developed by Pulliainen et al. (Pulliainen et al., 2020; Bronnimann et al., 2018; Brown et al., 2019). This dataset is from the

200   website of the Finnish Meteorological Institute (FMI) (https://www.globsnow.info/swe/archive_v3.0/auxiliary_data/). The

201   dataset provides data from 2687 distributed regional snow course observations and contains 343,241 SWE observational data

202   points from 1979 to 2018. The snow courses of the HSSC dataset are transects in which SWE is sampled manually at

203   multiple locations with typical conditions to eliminate uncertainty in the regional-scale spatial variability of SWE due to the

204   influence of snowpack characteristics and land cover type (Pulliainen et al., 2020).

205   We carefully screened the Russian snow survey data and HSSC data and eliminated some abnormal observational data to

206   ensure the high quality of the training, validation, and test sets. The null and zero values are removed during the HSSC data

207   screening process. The null values, negative numbers, and extreme SWE values greater than 2000 mm are removed during

208   the Russian snow survey data screening process.

209   **2.4.2 Accuracy evaluation method for datasets**

210   Mean absolute error (MAE), root mean square error (RMSE), Pearson's correlation coefficient (R), and coefficient of

211   determination (R^2) are used to evaluate the accuracies of AMSR-E/AMSR2 SWE, ERA-Interim SWE, GLDAS SWE,

212   GlobSnow SWE, ERA5-land SWE, multisource data-averaged SWE, and the RRM SWE product. The specific equation of

213   accuracy evaluation error is described as follows.

214 $$MAE = \frac{1}{n}\sum_{i=1}^{n}|f_i - y_i|, \qquad (2)$$

215 $$RMSE = \left[\frac{\sum_{i=1}^{n}(f_i - y_i)^2}{n}\right]^{\frac{1}{2}}, \qquad (3)$$

216 $$R = \frac{1}{n-1}\sum_{i=1}^{n}\left(\frac{f_i - \overline{f}}{\sigma_f}\right)\left(\frac{y_i - \overline{y}}{\sigma_y}\right), \qquad (4)$$

217 $$R^2 = \frac{\sum_{i=1}^{n}\left(f_i - \overline{y}\right)^2}{\sum_{i=1}^{n}\left(y_i - \overline{y}\right)^2}, \qquad (5)$$

218 where n is the number of samples in the validation dataset, f_i is the SWE dataset product, and y_i is the measured SWE at

219 the station. $\overline{f}$ and $\overline{y}$ are the averages of SWE products and measured SWEs, respectively. σ_f and σ_y are the standard

220 deviation of SWE products and measured SWEs, respectively.

221 To further evaluate the accuracy of the RRM SWE dataset at the spatial scale, we compared it with AMSR-E/AMSR2

222 SWE, ERA-Interim SWE, GLDAS SWE, GlobSnow SWE, and ERA5-Land SWE at different altitude gradients. We also

223 evaluated MAE, RMSE, R and R^2 separately for 11 elevation intervals: <100 m, 100-200 m, 200-300 m, 300-400 m, 400-

224 500 m, 500-600 m, 600-700 m, 700-800 m, 800-900 m, 900-1000 m, and >1000 m. In addition, we evaluated the

225 performances of the RRM SWE product in three representative regions: Russia, Canada, and Finland.

226 We used the Mann-Kendall trend test (Mann, 1945; Kendall, 1990) method to evaluate the variation trend in the RRM

227 SWE dataset from 1979 to 2019 and analyzed its reliability in terms of time series. Since the AMSR-E/AMSR2 SWE

228 product and the GlobSnow SWE product lack SWE data for Greenland, we removed the Greenland data to maintain

229 consistency in the spatial extent of the comparison data.

3 Results and discussion

3.1 Overall accuracy evaluation of the RRM SWE product

In this study, the accuracies of the RRM SWE, AMSR-E/AMSR2 SWE, ERA-Interim SWE, GLDAS SWE, GlobSnow SWE, and ERA5-land SWE were compared using test datasets from 2015 to 2018. MAE, RMSE, R, and R^2 were used to reflect the data quality of each SWE product. In addition, we compared the RRM SWE product with the SWE dataset obtained by the multisource data average method.

According to the verification results in Fig. 3 and Table 2, the RRM SWE data have the best overall accuracy, and the MAE, RMSE, R, and R² between the observed SWEs are 0.21, 25.37 mm, 0.89, and 0.79, respectively. The overall accuracy of the GlobSnow SWE and ERA5-land SWE products is higher than that of other SWE products. The overall deviation of the ERA5-land SWE products is the smallest except for the RRM SWE data, with MAE and RMSE values of 0.32 and 37.02 mm, respectively. The correlation between the ERA5-land SWE and observed SWE is the highest except for the RRM SWE data, with R and R² values of 0.84 and 0.71, respectively. Although the overall deviation between the GlobSnow SWE dataset and the measured SWE is small, its correlation with the measured value is low. The overall deviation between the ERA5-land SWE dataset and the measured SWE is higher than that of the GlobSnow SWE dataset, but its estimation accuracy for the high-value region of the SWE is low. In addition, the overall accuracy of the ERA-Interim SWE dataset and GLDAS SWE dataset is relatively low, but their integrities are higher than those of the GlobSnow SWE dataset and AMSR-E/AMSR2 SWE dataset in terms of temporal and spatial series. The AMSR-E/AMSR2 SWE dataset has a higher estimation accuracy for the low-value SWE region. Moreover, in the land region above 45° N, most of the existing SWE data products with regard to temporal and spatial degrees are missing to various degrees. Obviously, the accuracies of the existing SWE products were uneven, as no type of SWE dataset is perfect.

The verification results also indicate the following ranking orders:

The MAE ranking order is RRM SWE < GlobSnow SWE = ERA5-land SWE < ERA-Interim SWE < multisource data average SWE < AMSR-E/AMSR2 SWE < GLDAS SWE.

The RMSE ranking order is RRM SWE < ERA5-land SWE < GlobSnow SWE < ERA-Interim SWE < multisource data

254   average SWE < AMSR-E/AMSR2 SWE < GLDAS SWE.

255   The R ranking order is RRM SWE > ERA5-land SWE > GlobSnow SWE > ERA-Interim SWE > GLDAS SWE >

256 multisource data average SWE > AMSR-E/AMSR2 SWE.

257   The R^2 ranking order is RRM SWE > ERA5-land SWE > GlobSnow SWE > ERA-Interim SWE > GLDAS SWE >

258 multisource data average SWE > AMSR-E/AMSR2 SWE.

259   Compared with the ERA-Interim SWE, AMSR-E/AMSR2 SWE, GLDAS SWE, GlobSnow SWE, ERA5-land SWE, and

260 multisource data average SWE, the MAE of the RRM SWE and observed SWE is reduced by 0.22, 0.28, 0.37, 0.11, 0.11 and

261 0.23, respectively. The RMSE of the RRM SWE and observed SWE is reduced by 21.44 mm, 27.02 mm, 39.88 mm, 15.62

262 mm, 11.65 mm, and 26.63 mm, respectively. The correlation coefficients of the RRM SWE and observed SWE are improved

263 by 0.20, 0.42, 0.37, 0.19, 0.05, and 0.38, respectively. The coefficient of determination of the RRM SWE and observed SWE

264 is improved by 0.31, 0.57, 0.52, 0.30, 0.08, and 0.53, respectively. Although the multisource data average method can

265 improve the accuracy of SWE products to some extent (better than AMSR-E/AMSR2 SWE and GLDAS SWE), the

266 improvement of this method is still very limited. The RRM SWE product has a significant advantage over the multisource

267 data average method, and its accuracy is much higher than that of the simple multisource data average method (Table 2).

268 Based on the above verification results, the accuracy of the RRM SWE is significantly improved; the RRM SWE dataset has

269 higher accuracy than that of any single grid SWE dataset, and it also fills the gap in the original SWE data in terms of spatial

270 and temporal resolutions.

271   Based on the kernel density estimation method, we analyzed the density distribution of different SWE datasets (Fig. 4).

272 The results show that the RRM SWE dataset is closer to the 1:1 line and has the highest accuracy. The RRM SWE dataset is

273 particularly accurate for SWE estimation in the low-value region, and the test data are concentrated near the 1:1 line in the

274 high-density region (kernel density estimation > 0.00015) (Fig. 4). In contrast, the high-density regions of the GLDAS SWE

275 dataset, ERA-Interim SWE dataset, and AMSR-E/AMSR2 SWE dataset deviate significantly from the 1:1 line, resulting in

276 poor accuracy. The AMSR-E/AMSR2 SWE, GLDAS SWE, and GlobSnow SWE are underestimated relative to the SWE

277 measured at the site, among which GLDAS SWE underestimated the observed SWE the most seriously, while ERA5-land

278 SWE overestimated the observed SWE. Although the accuracies of GlobSnow SWE and ERA5-land SWE are relatively

279   high, their dispersion degrees are large (the kernel density estimation for most test data is less than 0.0001). Overall, the

280   RRM SWE data have a higher overall estimation accuracy, especially for the low-value area of SWE. For an SWE above

281   400 mm, the MAE and RMSE of the RRM SWE product and the measured SWE are 0.35 and 43.57 mm, respectively.

282   The estimation accuracy of the RRM SWE product for the high value range of SWE (SWE > 400 mm) is lower than that for

283   the low value range of SWE (SWE < 400 mm) (Fig. 4). The main reason for this is that the training accuracy of the RRM

284   model for the high-value range of SWE is affected by the small number of stations that observe the high-value range of

285   SWE.

286   However, in this study, there are still some uncertainties in the ridge regression machine learning algorithm that integrates

287   SWE products. First, this model is strongly dependent on on-site observational data, and the fusion precision of SWE is poor

288   in some areas with sparse observational stations. The fusion accuracy of SWE products will be affected to a certain extent

289   without considering the prior snow cover information. The RRM SWE product is still underestimated in cases of high SWE.

290   Then, in addition to the DEM, meteorological elements, NDVI, land type, and other factors will affect the SWE estimation.

291   Unfortunately, our current RRM presented here does not consider these factors as predictors, which is a limitation of the

292   current RRM SWE product. Finally, in complex terrain with an elevation interval >1000 m, the RRM SWE product

293   performed poorly, with an RMSE of 31.14 mm (Fig. 5), and the integration of SWE products remains challenging (Mortimer

294   et al., 2020).

295   **3.2 Accuracy evaluation of the RRM SWE product at different altitudes and regions**

296   The accuracy of each SWE product is not absolute at different altitude gradients based on evaluations of the AMSR-

297   E/AMSR2 SWE, ERA-Interim SWE, GLDAS SWE, GlobSnow SWE, and ERA5-land SWE product accuracies (Fig. 5).

298   The accuracy of a single SWE product is different from its overall accuracy. We consider the influence of altitude in the

299   algorithm and make full use of the accuracy advantage of each SWE data for different altitude gradients.

300   The above verification results show that the MAE, RMSE, R and R^2 between the RRM SWE product and measured SWE

301   perform well at altitude gradients of <100 m, 100-200 m, 200-300 m, 300-400 m, 400-500 m, 500-600 m, 600-700 m, 700-

302   800 m, 800-900 m, 900-1000 m and >1000 m (Fig. 5). Overall, the RRM SWE product has the highest accuracy in the

303 elevation intervals of <100 m, 100-200 m, 200-300 m, 400-500 m, 500-600 m, 600-700 m, 700-800 m, 800-900 m,

304 and >1000 m. The RRM SWE product itself has the best performance in the elevation interval <100 m. The ERA5-land

305 product has the best performance in the elevation interval 300-400 m. The GlobSnow product has the best performance in

306 the elevation interval 900-1000 m.

307 The RRM SWE product has good performance in different regions, and its RMSE in Russia, Canada, and Finland are

308 26.39 mm, 29.31 mm, and 25.29 mm, respectively; additionally, the performance of the RRM SWE product in different

309 regions is basically similar (Table 3). The RRM SWE product performs well not only at different altitudes but also in

310 different regions, and it has good stability.

311 **3.3 Comparison of spatial distribution patterns between the RRM SWE product and traditional SWE products**

312 A comparison of the spatially distributed annual average SWE distributions is made between the RRM SWE and AMSR-

313 E/AMSR2 SWE, ERA-Interim SWE, GLDAS SWE, GlobSnow SWE, and ERA5-land SWE in 2014, 2015, 2016, and 2017,

314 and their spatial distribution patterns are shown in Fig. 6.

315 Overall, the RRM SWE dataset, AMSR-E/AMSR2 SWE dataset, ERA-Interim SWE dataset, GLDAS SWE dataset,

316 GlobSnow SWE dataset, and ERA5-land SWE dataset have similar spatial distribution patterns in the land region above 45°

317 N, showing a trend of lower SWE in low latitudes and higher SWE in high latitudes. The AMSR-E/AMSR2 SWE dataset

318 covers a limited extent in the land region above 45° N, many data points are missing, and low SWE values exist at low

319 latitudes. In northern Siberia, the ERA-Interim SWE product has a higher SWE, and there are many abnormal, extreme SWE

320 values (SWE > 500 mm) in this dataset. In low-latitude regions, such as Alaska, North Siberia, and the easternmost region of

321 Russia, the SWE of GLDAS SWE products is significantly lower. The GlobSnow SWE product lacks SWE data for

322 Greenland, and this dataset has low SWEs in the Baffin Island, Koryak Mountains, Kamchatka Peninsula, and Alaska

323 regions. The ERA5-land SWE products have low SWEs in northeastern Russia, Scandinavia, and northeastern Canada. The

324 RRM SWE dataset is more reasonable for estimating the spatial distribution of SWE in the land region above 45° N, and the

325 data integrity is higher. Moreover, based on the new machine learning algorithm, a variety of SWE data products in different

326 time series are fused, which makes the RRM SWE dataset completely temporally and spatially continuous.

327   The relative difference between the RRM SWE data and GLDAS SWE data is the highest, and the relative difference is

328   greater than 80% in most low altitude regions (Fig. 7). The relative difference between the RRM SWE data and the

329   GlobSnow SWE data is relatively small overall, especially in most high-latitude areas where the relative difference is less

330   than 10% (Fig. 7). Overall, the annual average relative differences in the RRM SWE data and AMSR2 SWE, ERA-Interim

331   SWE, GLDAS SWE, GlobSnow SWE, and ERA5-land SWE are 37%, 41%, 54%, 25%, and 29%, respectively (Fig. 7).

332   Previous studies have shown that the accuracy of the SWE in the Northern Hemisphere estimated by GlobSnow SWE data is

333   higher (Pulliainen et al., 2020), while the spatial distribution pattern of the RRM SWE data is close to the estimation result of

334   GlobSnow SWE. In addition, the single point verification results based on the measured SWE data of meteorological stations

335   in section 3.1 show that the RRM SWE dataset has higher accuracy than the GlobSnow SWE dataset. The RRM SWE

336   dataset has good accuracy.

337 **3.4 Comparison of the annual variation tendencies of AMSR-E/AMSR2 SWE, ERA-Interim SWE, GLDAS SWE,**
338 **GlobSnow SWE, and ERA5-land SWE and the RRM SWE in the land region above 45° N**

339   Based on the Mann-Kendall trend test, we analyzed the changing trend in the region-wide annual average SWE of the

340   AMSR-E/AMSR2 SWE, ERA-Interim SWE, GLDAS SWE, GlobSnow SWE, ERA5-land SWE, and RRM SWE in the land

341   region above 45° N from 1979 to 2019.

342   Based on the Mann-Kendall trend test (see Fig. 8 and Table 4), from 1979 to 2019, the test value of the ERA-Interim

343   region-wide annual average SWE is 1.08, and there is no significant change trend under the significance test level of 0.05.

344   The test value of the GLDAS region-wide annual average SWE was 4.95 and showed a significant increasing trend at the

345   significance test level of 0.05. The test values of the AMSR-E/AMSR2 annual average SWE, GlobSnow annual average

346   SWE, ERA5-land annual average SWE, and RRM annual average SWE are -3.26, -2.54, -3.43, and -3.00, respectively, and

347   these four SWEs showed a significant decreasing trend at the significance test level of 0.05. Based on the analysis of the

348   RRM SWE product, between 1979 and 2019, the region-wide annual average SWE in the land region above 45° N decreased

349   by 15.1 percent. In the Northern Hemisphere, spring snow cover extent has decreased significantly, according to the Fifth

350   Assessment Report (AR5) of the IPCC. Between 1967 and 2010, the spring snow cover extent decreased by an average of

351 1.6 percent per decade, while the June snow cover extent decreased by 11.7 percent per decade (Stocker, 2014). Most studies

352 have shown that the annual variation tendency of snow depth and snow cover extent showed a significant decreasing trend in

353 the Northern Hemisphere (Brutel-Vuilmet et al., 2013), which is consistent with the annual variation tendency of the RRM

354 SWE dataset. This dataset can reflect the characteristics of snow cover change in the land region above 45° N in light of

355 climate change and can be used as the driving data for climate models to support climate change-related research. In

356 addition, this dataset is expected to provide a snow data basis for the study of "Arctic amplification".

357 **4 Data availability**

358 The RRM SWE product is available for free download from 'A Big Earth Data Platform for Three Poles'

359 (http://dx.doi.org/10.11888/Snow.tpdc.271556) (Li et al., 2021). The temporal resolution of the RRM SWE product is daily,

360 and the spatial resolution is 10 km. It spans latitudes of 45°N-90°N and longitudes of 180°W-180°E. A brief summary and

361 data description document (including data details, spatial range, and usage method) are also provided.

362 **5 Conclusions**

363 In this study, we propose a method to fuse multisource SWE data by a ridge regression model based on machine learning. A

364 new method was utilized to prepare a set of spatiotemporally seamless SWE datasets of the RRM SWE, combined with the

365 original AMSR-E/AMSR2 SWE, ERA-Interim SWE, GLDAS SWE, GlobSnow SWE, and ERA5-land SWE datasets. In the

366 RRM SWE dataset, the time series of the data is 1979-2019, the temporal resolution is daily, the spatial resolution is 10 km,

367 and the spatial range is the land region above 45° N.

368 The RRM SWE data product has the best accuracy, especially for the estimation of low SWE. The accuracy ranking of the

369 SWE dataset verified by the test dataset is described as follows: RRM SWE > ERA5-land SWE > GlobSnow SWE > ERA-

370 Interim SWE > multisource data average SWE > AMSR-E/AMSR2 SWE > GLDAS SWE. The accuracy of the RRM SWE

371 dataset is higher than that of the existing SWE products at most elevation intervals. The RRM SWE product has good

372 performance and stability in different regions. Moreover, the RRM SWE dataset spatiotemporally fills in the missing data of

the original SWE dataset.

Compared with traditional fusion methods, machine learning methods have a strong advantage. We find that the simple machine learning algorithm has not only high efficiency but also good accuracy in the preparation of SWE products on a global scale. Without losing the advantages of existing SWE products, this method can also make full use of station observational data to integrate the advantages of various SWE products. The model training process does not rely too much on a specific sample, and this model has a strong generalization ability. In addition, the influence of altitude on the preparation scheme is considered in detail in the model. Compared with the SWE dataset prepared by the traditional method, the spatial resolution is only 25 km, while this new method obtains an SWE dataset with a higher spatial resolution of 10 km.

We propose that the RRM SWE dataset preparation scheme has good continuity and can prepare real-time and high-quality SWE datasets in the land region above 45° N. In addition, the new method proposed in this paper has the advantages of simplicity and high precision in preparing large-scale SWE datasets and can be easily extended to the preparation of other snow datasets. This dataset is an important supplement to the land region above the 45° N SWE database and is expected to provide data support for Arctic cryosphere studies and global climate change studies.

Author contributions.

DS and HL designed the study and wrote the manuscript; JW, XH, and TC contributed to the discussions, edits, and revisions. DS and WJ compiled the model code.

Competing interests.

The authors declare that they have no conflicts of interest.

Acknowledgments.

The authors would like to thank the European Space Agency (ESA) for providing the GlobSnow data, the European Centre for Medium-Range Weather Forecasts (ECMWF) for ERA-Interim data and ERA5-land data, the National Aeronautics and

Space Administration (NASA) for the AMSR-E/AMSR2 data, the Goddard Earth Sciences Data and Information Services Center (GESDISC) for the GLDAS data, the Russian Federal Service for Hydrometeorology and Environmental Monitoring (ROSHYDROMET) for the snow survey data, and the Finnish Meteorological Institute (FMI) for the hemispheric-scale snow course (HSSC) observational data.

Financial support.

This research was supported by the Strategic Priority Research Program of the Chinese Academy of Sciences (Grant No. XDA19070302), the National Science Fund for Distinguished Young Scholars (Grant No. 42125604), and the National Natural Science Foundation of China (Grant No. 41971399, 41971325, 42171391).

References

Bair, E. H., Abreu Calfa, A., Rittger, K., and Dozier, J.: Using machine learning for real-time estimates of snow water equivalent in the watersheds of Afghanistan, The Cryosphere, 12, 1579-1594, 2018.

Balsamo, G., Albergel, C., Beljaars, A., Boussetta, S., Brun, E., Cloke, H., Dee, D., Dutra, E., Munoz-Sabater, J., Pappenberger, F., de Rosnay, P., Stockdale, T., and Vitart, F.: ERA-Interim/Land: a global land surface reanalysis data set, Hydrol Earth Syst Sc, 19, 389-407, 10.5194/hess-19-389-2015, 2015.

Barnett, T. P., Adam, J. C., and Lettenmaier, D. P.: Potential impacts of a warming climate on water availability in snow-dominated regions, Nature, 438, 303-309, 10.1038/nature04141, 2005.

Bintanja, R. and Andry, O.: Towards a rain-dominated Arctic, Nat Clim Change, 7, 263-+, 10.1038/Nclimate3240, 2017.

Bronnimann, S., Allan, R., Atkinson, C., Buizza, R., Bulygina, O., Dahlgren, P., Dee, D., Dunn, R., Gomes, P., John, V. O., Jourdain, S., Haimberger, L., Hersbach, H., Kennedy, J., Poli, P., Pulliainen, J., Rayner, N., Saunders, R., Schulz, J., Sterin, A., Stickler, A., Titchner, H., Valente, M. A., Ventura, C., and Wilkinson, C.: Observations for Reanalyses, Bulletin of the American Meteorological Society, 99, 1851-1866, 10.1175/Bams-D-17-0229.1, 2018.

Brown, R. D., Fang, B., and Mudryk, L.: Update of Canadian historical snow survey data and analysis of snow water

416   equivalent trends, 1967–2016, Atmosphere-Ocean, 57, 149-156, 2019.

417   Broxton, P. D., Van Leeuwen, W. J., and Biederman, J. A.: Improving snow water equivalent maps with machine learning of

418   snow survey and lidar measurements, Water Resources Research, 55, 3739-3757, 2019.

419   Brutel-Vuilmet, C., Menegoz, M., and Krinner, G.: An analysis of present and future seasonal Northern Hemisphere land

420   snow cover simulated by CMIP5 coupled climate models, Cryosphere, 7, 67-80, 10.5194/tc-7-67-2013, 2013.

421   Bulygina, O. N., Groisman, P. Y., Razuvaev, V. N., and Korshunova, N. N.: Changes in snow cover characteristics over

422   Northern Eurasia since 1966, Environmental Research Letters, 6, Artn 04520410.1088/1748-9326/6/4/045204, 2011.

423   Dee, D. P., Uppala, S. M., Simmons, A., Berrisford, P., Poli, P., Kobayashi, S., Andrae, U., Balmaseda, M., Balsamo, G., and

424   Bauer, d. P.: The ERA‐Interim reanalysis: Configuration and performance of the data assimilation system, Quarterly

425   Journal of the royal meteorological society, 137, 553-597, 2011.

426   Duzan, H. and Shariff, N. S. B. M.: Ridge regression for solving the multicollinearity problem: review of methods and

427   models, Journal of Applied Science, 2015.

428   Friedman, J., Hastie, T., and Tibshirani, R.: Regularization Paths for Generalized Linear Models via Coordinate Descent, J

429   Stat Softw, 33, 1-22, DOI 10.18637/jss.v033.i01, 2010.

430   Gelaro, R., McCarty, W., Suarez, M. J., Todling, R., Molod, A., Takacs, L., Randles, C. A., Darmenov, A., Bosilovich, M. G.,

431   Reichle, R., Wargan, K., Coy, L., Cullather, R., Draper, C., Akella, S., Buchard, V., Conaty, A., da Silva, A. M., Gu, W., Kim,

432   G. K., Koster, R., Lucchesi, R., Merkova, D., Nielsen, J. E., Partyka, G., Pawson, S., Putman, W., Rienecker, M., Schubert,

433   S. D., Sienkiewicz, M., and Zhao, B.: The Modern-Era Retrospective Analysis for Research and Applications, Version 2

434   (MERRA-2), J Climate, 30, 5419-5454, 10.1175/Jcli-D-16-0758.1, 2017.

435   Guilkey, D. K. and Murphy, J. L.: Directed Ridge Regression Techniques in Cases of Multicollinearity, J Am Stat Assoc, 70,

436   769-775, 1975.

437   Henderson, G. R., Peings, Y., Furtado, J. C., and Kushner, P. J.: Snow-atmosphere coupling in the Northern Hemisphere, Nat

438   Clim Change, 8, 954-+, 10.1038/s41558-018-0295-6, 2018.

439   Hoerl, A. E. and Kennard, R. W.: Ridge regression: applications to nonorthogonal problems, Technometrics, 12, 69-82,

440   1970a.

441 Hoerl, A. E. and Kennard, R. W.: Ridge regression: Biased estimation for nonorthogonal problems, Technometrics, 12, 55-

442 67, 1970b.

443 Imaoka, K., Kachi, M., Fujii, H., Murakami, H., Hori, M., Ono, A., Igarashi, T., Nakagawa, K., Oki, T., Honda, Y., and

444 Shimoda, H.: Global Change Observation Mission (GCOM) for Monitoring Carbon, Water Cycles, and Climate Change, P

445 Ieee, 98, 717-734, 10.1109/Jproc.2009.2036869, 2010.

446 IPCC, 2021: Climate Change 2021: The Physical Science Basis. Contribution of Working Group I to the Sixth Assessment

447 Report of the Intergovernmental Panel on Climate Change [Masson-Delmotte, V., P. Zhai, A. Pirani, S.L. Connors, C. Péan,

448 S. Berger, N. Caud, Y. Chen, L. Goldfarb, M.I. Gomis, M. Huang, K. Leitzell, E. Lonnoy, J.B.R. Matthews, T.K. Maycock,

449 T. Waterfield, O. Yelekçi, R. Yu, and B. Zhou (eds.)]. Cambridge University Press. In Press.

450 Kelly, R.: The AMSR-E Snow Depth Algorithm: Description and Initial Results, 2009.

451 Kendall, M. G.: Rank Correlation Methods, British Journal of Psychology, 25, 86–91, 1990.

452 Li, H., Shao, D., Li, H., Wang, W., Ma, Y., and Lei, H.: Arctic Snow Water Equivalent Grid Dataset (1979-2019), A Big

453 Earth Data Platform for Three Poles [dataset], 10.11888/Snow.tpdc.271556, 2021.

454 Luojus, K., Pulliainen, J., Takala, M., Lemmetyinen, J., Mortimer, C., Derksen, C., Mudryk, L., Moisander, M., Hiltunen,

455 M., and Smolander, T.: GlobSnow v3. 0 Northern Hemisphere snow water equivalent dataset, Scientific Data, 8, 1-16, 2021.

456 Mann, H. B.: Nonparametric test against trend, Econometrica, 13, 245-259, 1945.

457 Menne, M., Durre, I., Korzeniewski, B., McNeal, S., Thomas, K., Yin, X., Anthony, S., Ray, R., Vose, R., and Gleason, B.:

458 Global Historical Climatology Network–Daily (GHCN-Daily), Version, 3, V5D21VHZ, 2016.

459 Mortimer, C., Mudryk, L., Derksen, C., Luojus, K., Brown, R., Kelly, R., and Tedesco, M.: Evaluation of long-term Northern

460 Hemisphere snow water equivalent products, The Cryosphere, 14, 1579-1594, 2020.

461 Mudryk, L., Derksen, C., Kushner, P., and Brown, R.: Characterization of Northern Hemisphere snow water equivalent

462 datasets, 1981–2010, Journal of Climate, 28, 8037-8051, 2015a.

463 Mudryk, L. R., Derksen, C., Kushner, P. J., and Brown, R.: Characterization of Northern Hemisphere Snow Water Equivalent

464 Datasets, 1981-2010, J Climate, 28, 8037-8051, 10.1175/Jcli-D-15-0229.1, 2015b.

465 Muñoz Sabater, J.: ERA5-Land hourly data from 1981 to present, Copernicus Climate Change Service (C3S) Climate Data

Store (CDS), 2019.

Ntokas, K. F., Odry, J., Boucher, M.-A., and Garnaud, C.: Investigating ANN architectures and training to estimate snow water equivalent from snow depth, Hydrology and Earth System Sciences, 25, 3017-3040, 2021.

Pan, M., Fisher, C. K., Chaney, N. W., Zhan, W., Crow, W. T., Aires, F., Entekhabi, D., and Wood, E. F.: Triple collocation: Beyond three estimates and separation of structural/non-structural errors, Remote Sens Environ, 171, 299-310, 10.1016/j.rse.2015.10.028, 2015.

Pan, M., Sheffield, J., Wood, E. F., Mitchell, K. E., Houser, P. R., Schaake, J. C., Robock, A., Lohmann, D., Cosgrove, B., and Duan, Q.: Snow process modeling in the North American Land Data Assimilation System (NLDAS): 2. Evaluation of model simulated snow water equivalent, Journal of Geophysical Research: Atmospheres, 108, 2003.

Pulliainen, J.: Mapping of snow water equivalent and snow depth in boreal and sub-arctic zones by assimilating space-borne microwave radiometer data and ground-based observations, Remote Sens Environ, 101, 257-269, 10.1016/j.rse.2006.01.002, 2006.

Pulliainen, J., Luojus, K., Derksen, C., Mudryk, L., Lemmetyinen, J., Salminen, M., Ikonen, J., Takala, M., Cohen, J., Smolander, T., and Norberg, J.: Patterns and trends of Northern Hemisphere snow mass from 1980 to 2018 (vol 41, pg 861, 2020), Nature, 582, E18-E18, 10.1038/s41586-020-2416-4, 2020.

Reichle, R. H., Koster, R. D., De Lannoy, G. J. M., Forman, B. A., Liu, Q., Mahanama, S. P. P., and Toure, A.: Assessment and Enhancement of MERRA Land Surface Hydrology Estimates, J Climate, 24, 6322-6338, 10.1175/Jcli-D-10-05033.1, 2011.

Rodell, M., Houser, P., Jambor, U., Gottschalck, J., Mitchell, K., Meng, C.-J., Arsenault, K., Cosgrove, B., Radakovich, J., and Bosilovich, M.: The global land data assimilation system, Bulletin of the American Meteorological Society, 85, 381-394, 2004.

Saleh, A. M. E., Arashi, M., and Kibria, B. G.: Theory of ridge regression estimation with applications, John Wiley & Sons2019.

Santi, E., Brogioni, M., Leduc-Leballeur, M., Macelloni, G., Montomoli, F., Pampaloni, P., Lemmetyinen, J., Cohen, J., Rott, H., and Nagler, T.: Exploiting the ANN Potential in Estimating Snow Depth and Snow Water Equivalent From the Airborne

491   SnowSAR Data at X-and Ku-Bands, IEEE Transactions on Geoscience and Remote Sensing, 2021.

492   Snauffer, A. M., Hsieh, W. W., and Cannon, A. J.: Comparison of gridded snow water equivalent products with in situ

493   measurements in British Columbia, Canada, J Hydrol, 541, 714-726, 10.1016/j.jhydrol.2016.07.027, 2016.

494   Snauffer, A. M., Hsieh, W. W., Cannon, A. J., and Schnorbus, M. A.: Improving gridded snow water equivalent products in

495   British Columbia, Canada: multi-source data fusion by neural network models, Cryosphere, 12, 891-905, 10.5194/tc-12-891-

496   2018, 2018.

497   Stocker, T.: Climate change 2013: the physical science basis: Working Group I contribution to the Fifth assessment report of

498   the Intergovernmental Panel on Climate Change, Cambridge university press2014.

499   Tedesco, M. and Jeyaratnam, J.: AMSR-E/AMSR2 Unified L3 Global Daily 25 km EASE-Grid Snow Water Equivalent,

500   Version 1.[online] Boulder, Colorado USA, NASA National Snow and Ice Data Center Distributed Active Archive Center,

501   2019.

502   Vuyovich, C. M., Jacobs, J. M., and Daly, S. F.: Comparison of passive microwave and modeled estimates of total watershed

503   SWE in the continental U nited S tates, Water resources research, 50, 9088-9102, 2014.

504   Walker, A., Brasnett, B., and Brown, R.: Canadian Meteorological Centre (CMC) daily gridded snow depth analysis for

505   Northern Hemisphere, 1998-2008, 2011.

506   Wang, J. W., Yuan, Q. Q., Shen, H. F., Liu, T. T., Li, T. W., Yue, L. W., Shi, X. G., and Zhang, L. P.: Estimating snow depth

507   by combining satellite data and ground-based observations over Alaska: A deep learning approach, J Hydrol, 585, ARTN

508   12482810.1016/j.jhydrol.2020.124828, 2020.

509   Xiao, X. X., Zhang, T. J., Zhong, X. Y., Shao, W. W., and Li, X. D.: Support vector regression snow-depth retrieval algorithm

510   using passive microwave remote sensing data, Remote Sens Environ, 210, 48-64, 10.1016/j.rse.2018.03.008, 2018.

511
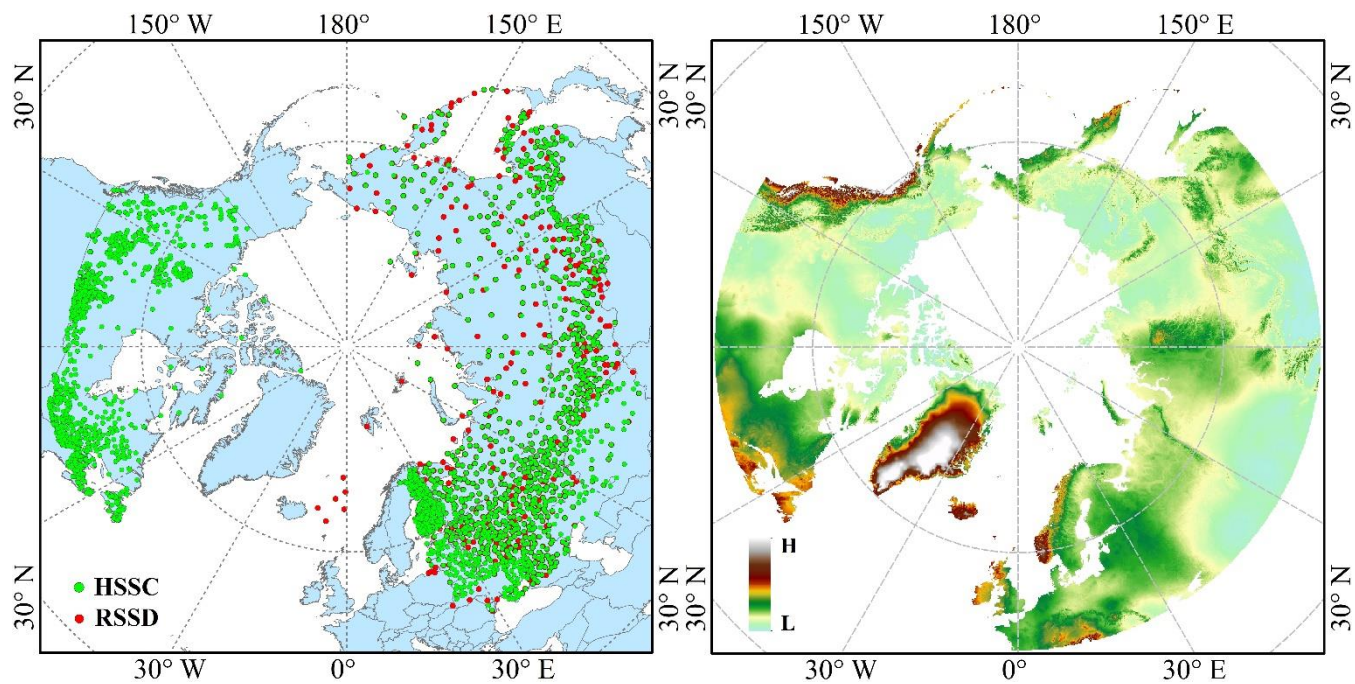
512

513 **Figure 1: The DEM and snow survey stations of the research region. The right subgraph shows the DEM, and the left subgraph**

514 **shows the SWE observational stations. HSSC, hemispheric-scale snow course; RSSD, the Russian snow survey station. The spatial**

515 **range of the RRM SWE product is consistent with that of the DEM.**

516

517

518   **Table 1: Introduction to the SWE data.**

Data type	Data name	Time series	Temporal resolution	Spatial resolution	Spatial coverage	File format
Remote sensing data	AMSR-E/AMSR2	2002-2011/2012-2020	Daily	25 km x 25 km	Global (No Greenland)	HDF5
Data assimilation dataset	GLDAS	1979-2020	Daily	0.25°×0.25°	Global	NetCDF
	GlobSnow	1979-2018	Daily	0.25°×0.25°	Northern Hemisphere (No Greenland)	NetCDF
Reanalysis dataset	ERA-Interim	1979-2019	Daily	0.25°×0.25°	Global	NetCDF
	ERA5-land	1981- present	Hour	0.1°×0.1°	Global	NetCDF

519
520
521

522
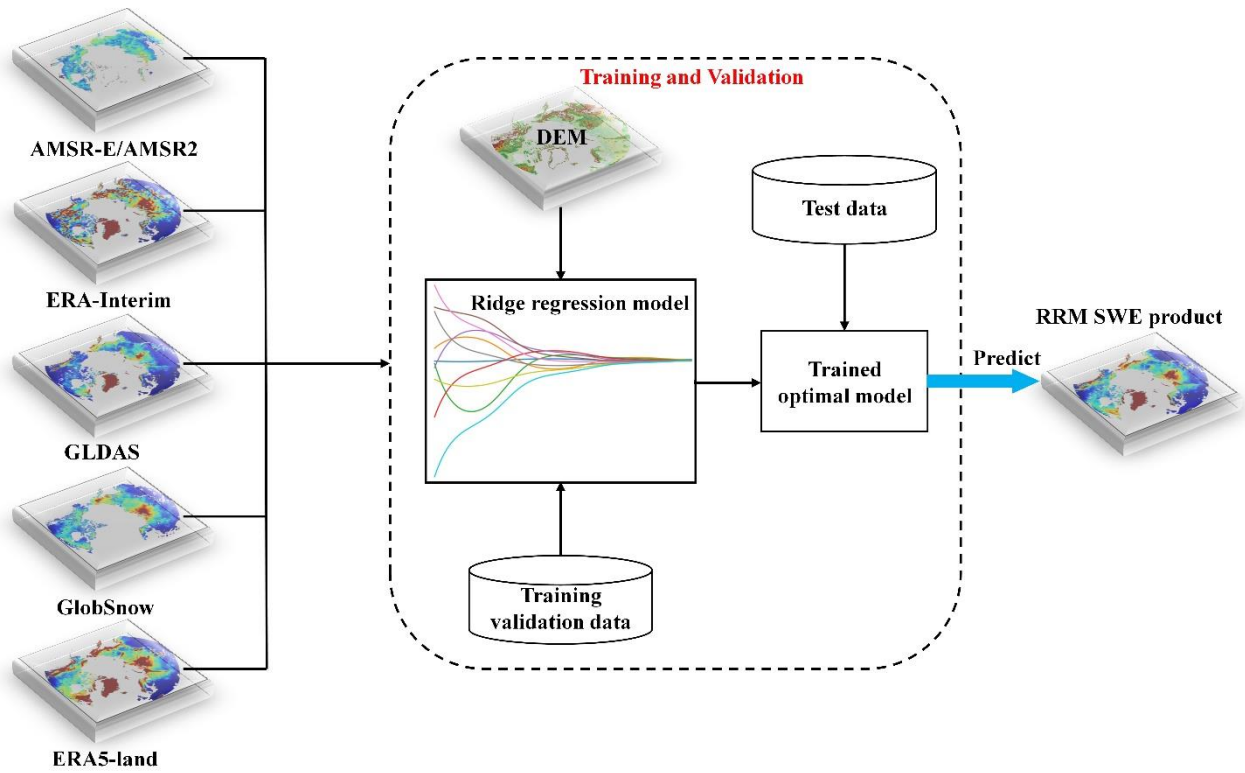
Figure 2: Flow chart of the RRM SWE data preparation (preparation of spatiotemporal seamless SWE datasets mainly includes

three processes: model training, model reasoning, and SWE data preparation).

525

526

527 **Table 2: Error list for the station data and grid snow water equivalent products.**

Error type	MAE	RMSE (mm)	R	R^2
ERA-Interim	0.43	46.81	0.69	0.48
AMSR-E/AMSR2	0.49	52.39	0.47	0.22
GLDAS	0.58	65.25	0.52	0.27
GlobSnow	0.32	40.99	0.70	0.49
ERA5-land	0.32	37.02	0.84	0.71
Multisource data average	0.44	52.00	0.51	0.26
RRM SWE	0.21	25.37	0.89	0.79

528
529

530
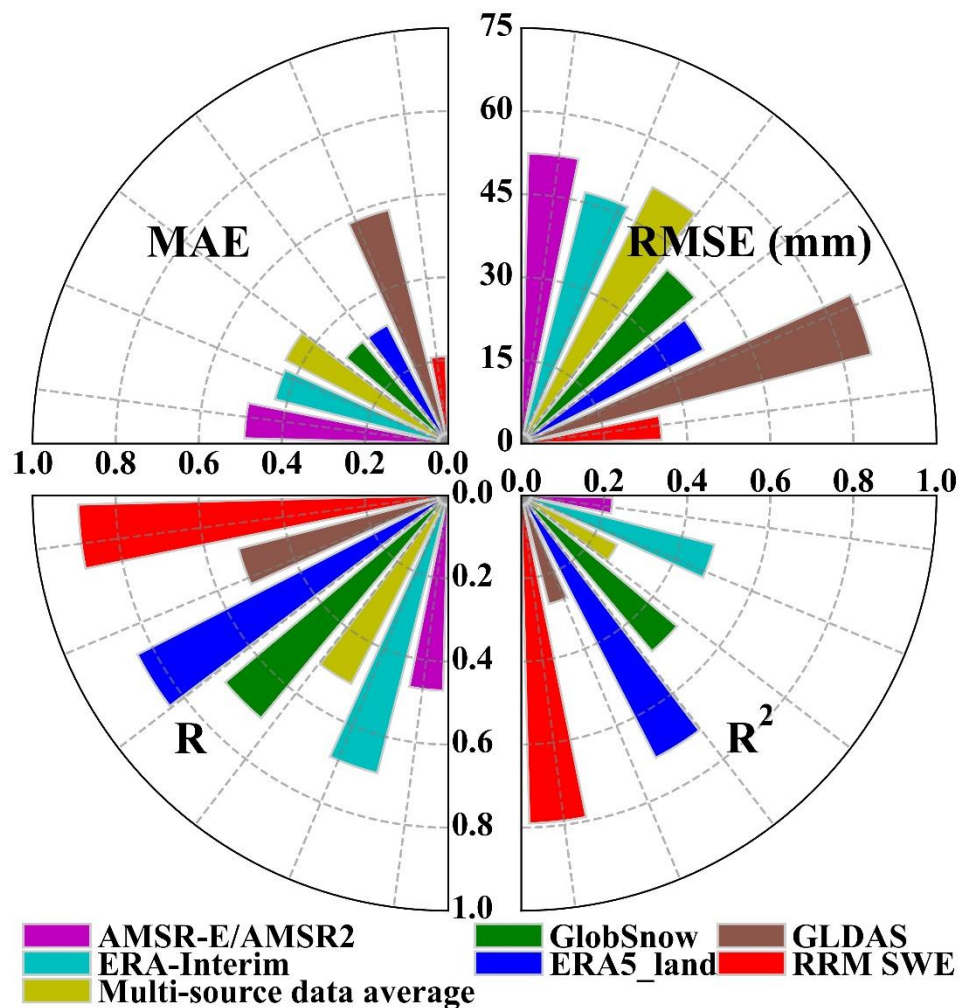
Figure 3: Accuracy comparison of various SWE products. The upper left sector represents the MAE, the upper right sector represents the RMSE, the lower left sector represents R, and the lower right sector represents R². The sector axis represents the size of the error, and the color represents different SWE datasets.

534
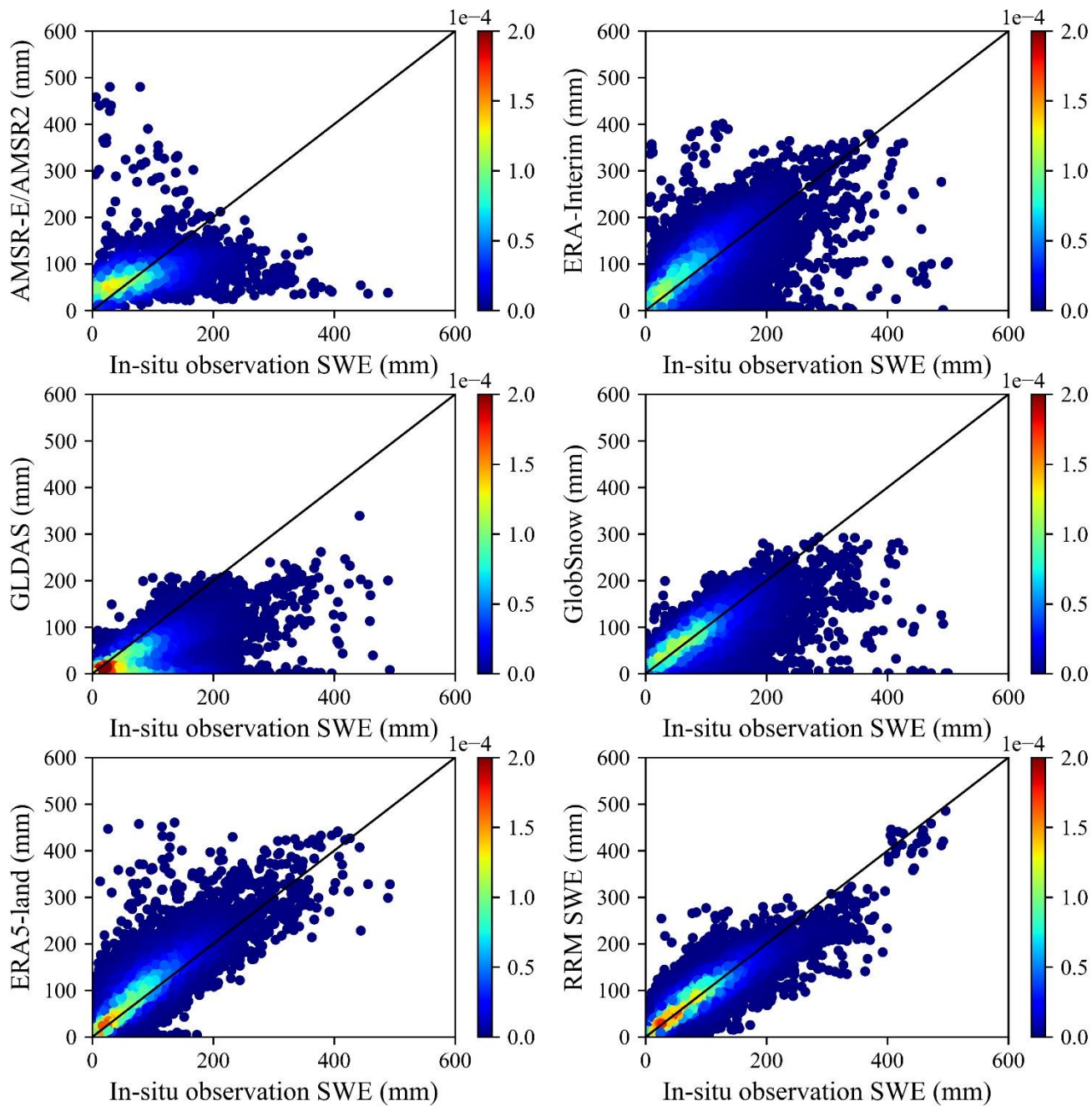
Figure 4: Error verification density diagram (a total of 38807 sample points were used for verification). The color bar represents the value of kernel density estimation. The closer the high-density area is to the 1:1 line, the higher the verification accuracy of the dataset is at most of the measuring stations.
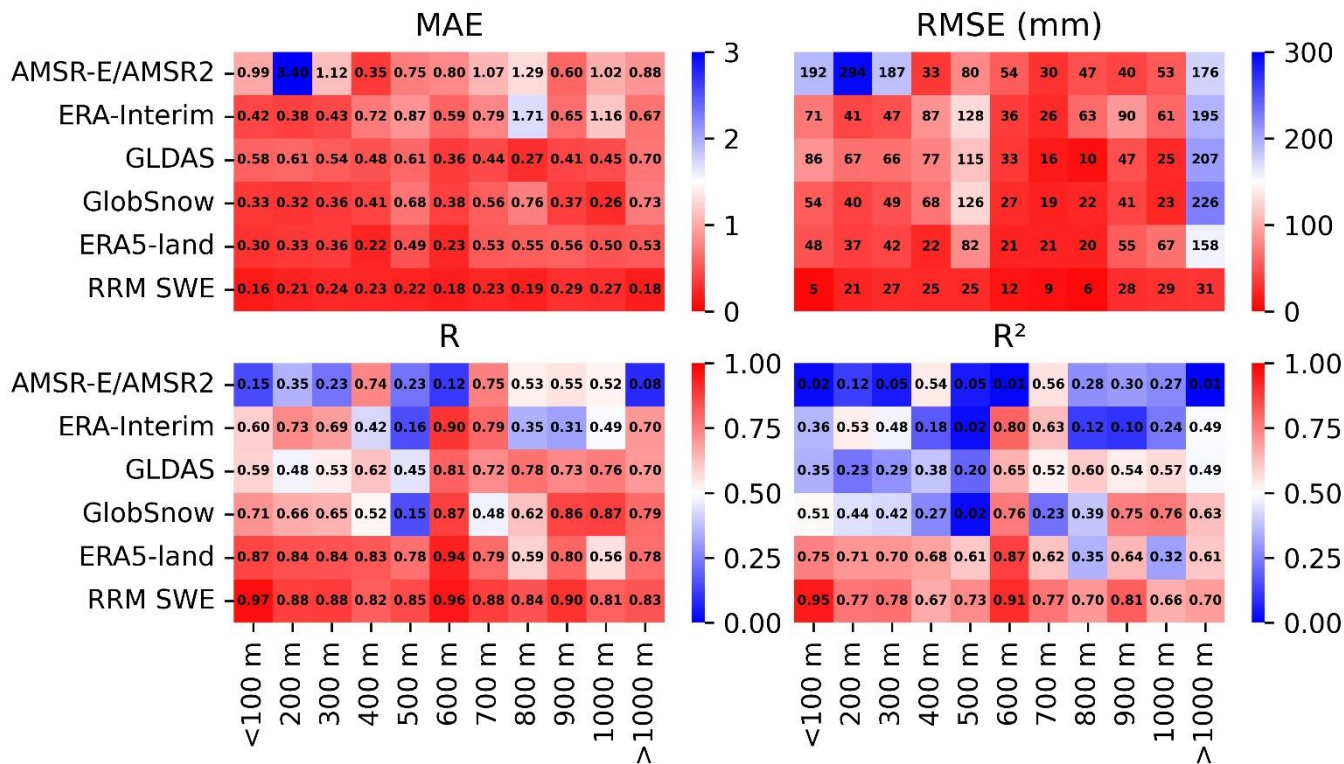
Figure 5: Comparison of the error between the RRM SWE and AMSR-E/AMSR2 SWE, ERA-Interim SWE, GLDAS SWE, GlobSnow SWE, and ERA5-land SWE at different altitudes (the abscissa represents the altitude gradient, and the ordinate represents different SWE datasets). The color bar indicates the error in each SWE dataset. The closer to red the color is, the higher the accuracy is. MAE: mean absolute error, RMSE: root mean square error, R: Pearson's correlation coefficient, R^2: coefficient of determination).

555   **Table 3: Error list for the station data and RRM SWE product in different regions.**

Region	MAE	RMSE (mm)	R	R^2
Russia	0.20	26.39	0.89	0.79
Canada	0.23	29.31	0.87	0.76
Finland	0.21	25.29	0.89	0.79

556

557
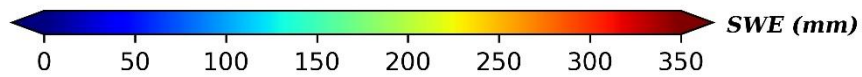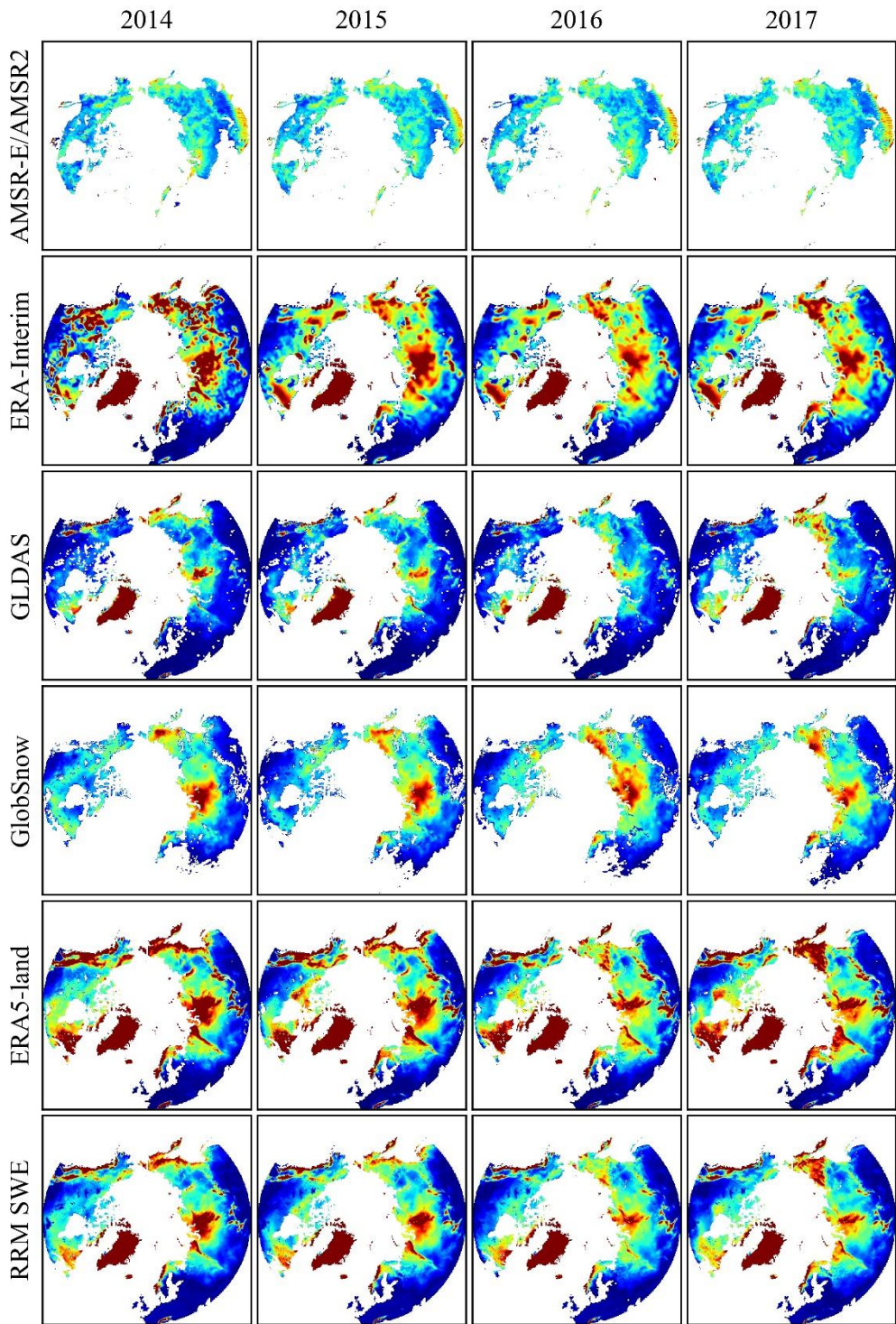
558   **Figure 6: Comparison of the spatial distribution characteristics between the RRM SWE and AMSR-E/AMSR2 SWE, ERA-**

559   **Interim SWE, GLDAS SWE, GlobSnow SWE, and ERA5-land SWE (the four columns of images represent the comparison results**

560   **in 2014, 2015, 2016, and 2017, respectively).**

561
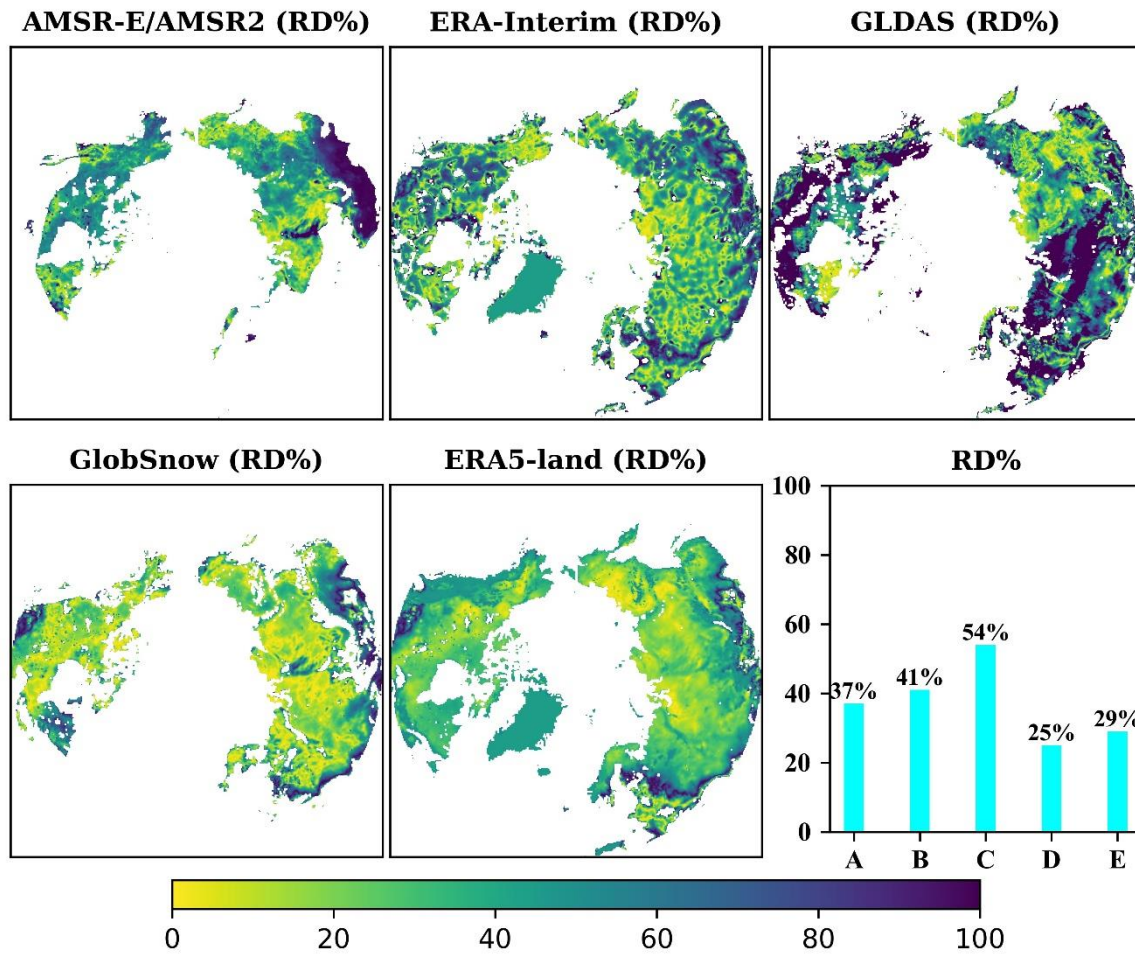
Figure 7: Temporal and spatial distributions of relative differences (RD%) between the RRM SWE and AMSR-E/AMSR2 SWE, ERA-Interim SWE, GLDAS SWE, GlobSnow SWE, and ERA5-land SWE. Lower-right subgraph: Comparison of annual average relative differences between the RRM SWE and AMSR2 SWE (A), ERA-Interim SWE (B), GLDAS SWE (C), GlobSnow SWE (D), and ERA5-land SWE (E).

567
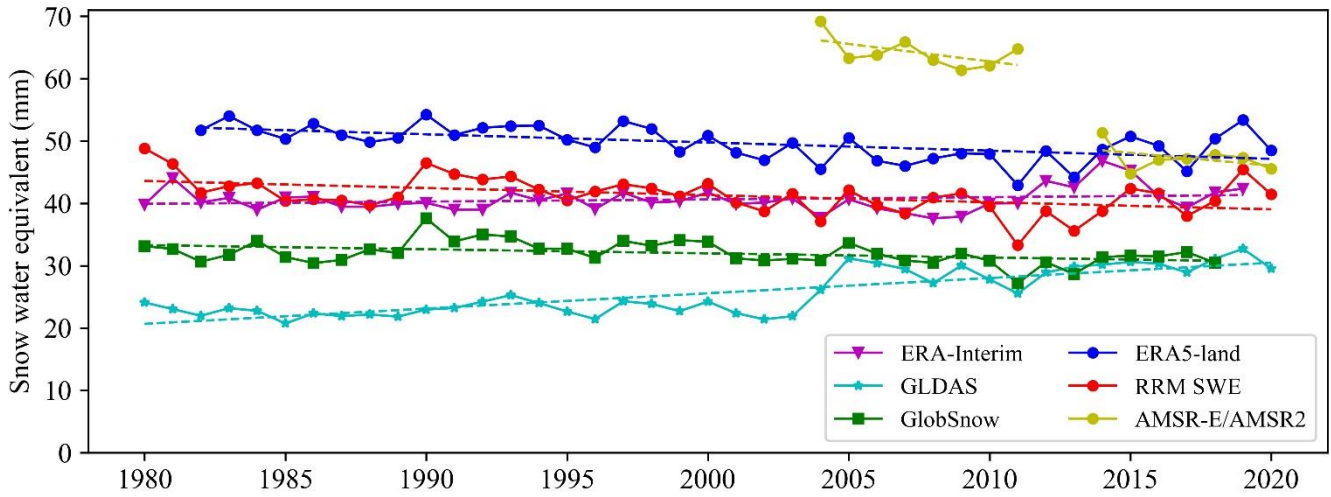
Figure 8: Annual variation tendency in the AMSR-E/AMSR2 SWE, ERA-Interim SWE, GLDAS SWE, GlobSnow SWE, ERA5-land SWE and RRM SWE products from 1979 to 2019 (the dotted line is the trend line calculated based on the Mann-Kendall method).

572   **Table 4: Results of the Mann-Kendall trend test performed for various snow water equivalent products from 1979 to 2019.**

Data	P value	Test value	Trend
AMSR-E/AMSR2	0.00	-3.26	Decreasing
ERA-Interim	0.27	1.08	No trend
GLDAS	7.29e-07	4.95	Increasing
GlobSnow	0.01	-2.54	Decreasing
ERA5-land	0.00	-3.43	Decreasing
RRM SWE	0.00	-3.00	Decreasing

573   *Significance level alpha = 0.05